5-1-1978

Production and Evaluation of a Holographic Lens

H. Scott Gregory

PHOTOGRAPHIC SCIENCE AND INSTRUMENTATION

PRODUCTION AND EVALUATION OF A HOLOGRAPHIC LENS

by

H. Scott Gregory, Jr.

A thesis submitted in partial fulfillment of the requirements for the degree of Bachelor of Science in the School of Photographic Arts and Sciences in the College of Graphic Arts and Photography of the Rochester Institute of Technology

May, 1978

Thesis Advisor: Professor M. Aboulata

ACKNOWLEDGEMENTS

I would especially like to acknowledge my thesis advisor, Professor Mohamed Abouelata, for the tremendous educational and moral support he has given throughout this project.

In addition, I would like to thank Dr. R. Francis for donating the spectroscopic plates and Professor J. Carson for providing most of the needed apparatus. I would also like to thank the entire R.I.T. Photographic Science Department for the opportunity of furthering my education in this very interesting field of study.

TABLE OF CONTENTS

LIST OF FIGURES

ABSTRACT

This thesis is concerned with the production of high diffraction efficiency holographic lenses for laser machining. A holographic lens is a high efficiency, low absorption phase hologram which, in this application, is used to diffract an expanded, highpower laser beam into a desired focal point or pattern. For ideal phase holograms, the coupled-wave theory, as applied by H. Kogelnik[1], predicts diffraction efficiencies as high as 100%. This implies that all the power in the expanded laser beam could be diffracted into the focal point or pattern.

Single focal point holographic lenses have been produced with 40% diffraction efficiency. These lenses were produced by reversal bleaching Kodak type 649F spectroscopic plates. 50% diffraction efficiency has been obtained with holographic lenses which have a focal pattern. These lenses were constructed on Agfa type 8E75 Scientia plates using a modified reversal bleach process.

INTRODUCTION

Since the development of the high-power laser, industry has come to realize its usefulness as a tool for precision machining operations. They can be used to cut, weld, or drill with great accuracy. For these purposes high-power lasers are focussed through conventional optical systems to the desired focal point where the machining operation is to be performed. If multiple machining operations are to be performed on a single part, the laser or part has to be moved to the location for the successive machining operation. For these purposes the computer has found a variety of applications. An alternate method of performing several machining operations on a single part would be to have a holographic lens focus the high-power laser into the desired pattern at one time.

A holographic lens or holographic optical element (HOE), as it is more commonly known, is a high efficiency hologram which is used to diffract light into a desired area. If a hologram of a point source or an array of point sources is constructed in the usual manner and then reconstructed with a reference wave which is conjugate to the constructing reference wave, the hologram will focus the reconstruction reference wave into a point or an array of points. If the reconstruction wave was produced by a high-power laser, a machining operation could be performed at the focal point or

pattern of the holographic lens. These lenses could eliminate the expensive equipment which is presently used to do multiple machining operations. They have the additional advantage of being relatively simple and economic to produce.

It has been demonstrated that low absorption phase holograms can withstand energy densities of up to 20 joules per square centimeter[2]. This means a holographic lens, with a clear aperture of 12 x 12 square centimeters, could be irradiated with 2880 joules of energy. If the lens has a high diffraction efficiency, which is the ratio of the power incident on the lens to the power diffracted into the desired area, a large portion of the 2880 joules would be available for laser machining. This would be more than enough energy to perform a multiple machining operation. This operation would be limited only by the pulse duration and the area of the focal pattern.

In 1971, it was demonstrated by J. M. Moran, of Bell Labs, that holographic lenses could be produced for laser machining. He was able to use these lenses to machine single and multiple spots in a .12μm thin film of tantalum deposited on glass. Spot sizes as small as 14μm in diameter were obtained with lens diffraction efficiencies of 30%.

In 1977, E. Schwartz[3] did his senior research thesis at RIT in this area. He had hoped to produce a holographic lens of higher diffraction efficiency. But due to problems associated with his procedure, he was only able to obtain

diffraction efficiencies of 28%.

This research has produced a holographic lens which has 50% diffraction efficiency. This would be enough efficiency to make a holographic lens highly feasible for improving laser machining operations.

THEORY

Holography is more specifically known as wavefront reconstruction. A hologram is the record of an irradiance pattern caused by the interaction of two highly coherent light waves. The two waves are referred to as the reference wave and signal wave. As with the interaction of any two waves, constructive interference occurs when the two waves are in phase and destructive interference occurs when the two waves are out of phase. When the two waves are highly coherent light waves, the constructive interference is manifested by light irradiance and the destructive interference is characterized by a lack of light irradiance. The equation for the irradiance[4] "E" which results from this interference is given by Equ.(1).

$$\vec{E} = \vec{E}_r + \vec{E}_s + 2\vec{a}_r \cdot \vec{a}_s \cos(\theta_r - \theta_s) \qquad (1)$$

If this irradiance pattern, which corresponds to the shape of the two construction wavefronts, is recorded by a photosensitive medium, a diffraction grating or hologram is created. This hologram can generate the signal wavefront if it is irradiated by the reference wavefront.

Diffraction occurs when the wave normals are bent by encountering obstacles whose optical transmission or reflection properties change in distances approaching the wavelength of the irradiating light. Holograms can be classified as behaving like plane diffraction gratings or volume diffraction

gratings. A plane diffraction grating is shown, on-edge, in Fig. 1. The grating may consist of a set of periodically spaced transparent slits in an opaque screen. When a plane wave is incident on the grating, the condition determining the in-phase or constructive interference is given by Equ. (2).

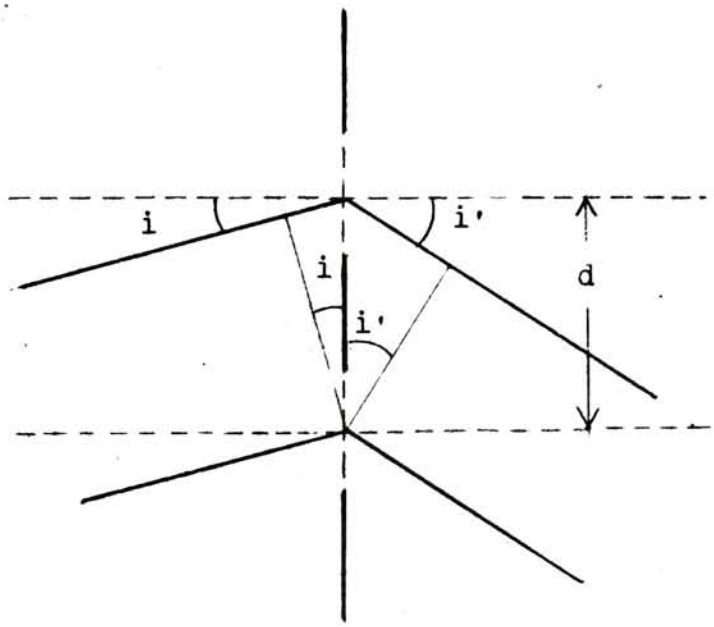

Fig. 1. Plane diffraction grating

$$d(\sin i + \sin i') = n\lambda \qquad (2)$$

This is the well known "grating equation", where d is the grating spacing, i is the angle of incidence, i' is the angle of diffraction, and n is the order of diffraction (n = 1 is first order diffraction).

Fig. 2 shows a volume diffraction grating, edge-on, which is irradiated with a plane wave and consists of

periodically spaced scattering planes.

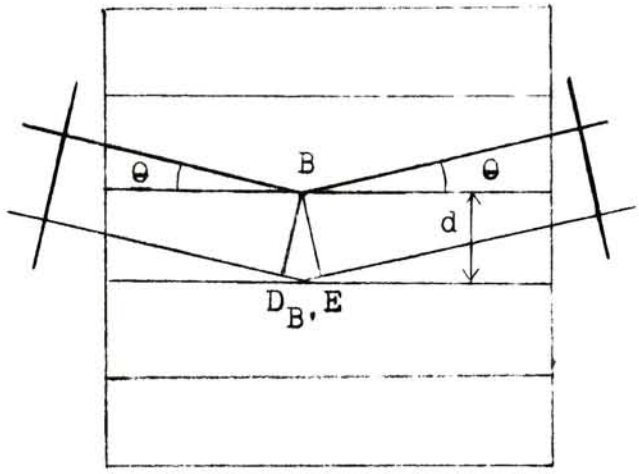

Fig. 2. Volume diffraction grating

As with plane diffraction gratings, the same principle of in-phase addition of light scattered by sucessive planes to obtain maximum output is applied here, with the result that

$$DB' + B'E = 2\ d\ \sin\theta = \lambda \qquad (3)$$

is the equation determining the constructive interference and diffraction of a plane wave. Equ. (3) is called Bragg's law after W. L. Bragg[5] who derived it for X-ray diffraction from atomic planes in a crystal. Bragg assumed that diffraction from the crystal was actually a reflection of incident waves from the crystal planes. Maximum diffraction occurs when the grazing angles of incidence and reflection are equal, as is shown in Fig. 2, and given by θ in Equ. (3).

Comparison of Equ. (2) and Equ. (3) reveals that the

latter is a more sensitive criterion for observing maximum diffraction. For volume gratings, once the incident angle is chosen, the wavelength and the diffraction angle are determined. This is not the case for plane gratings. Equ. (2) allows for arbitrary choice of both angle of incidence and wavelength (within the limitation that $|\sin i|$ and $|\sin i'| \leq 1$). It is therefore necessary to look at diffraction by a volume grating.

There are two types of volume diffraction gratings which can be formed in photo-sensitive medium. One is an absorption hologram, the other is a phase hologram. The absorption hologram is produced when the photo-sensitive medium is processed to give density in the form of silver metal. This acts to diffract the light by selectively changing the transmittance of the incident light. If the same hologram is bleached, so as to convert the silver metal to a transparent compound whose index of refraction differs from that of the gelatin, then the record is written in the resulting localized changes in index of refraction of the emulsion. The hologram is called a phase hologram. For phase holograms, the spatial phase modulation imposed on a wave as it passes through the hologram is made to correspond to the recorded diffraction pattern. Because the volume, phase holograms have low absorption of the incident wave, they can closely approximate an ideal volume diffraction grating.

Most analyses of volume holograms succeed in predicting

the observed angular and wavelength selectivity. The coupled-wave theory is capable of not only predicting the selective response of the volume hologram but also carries these predictions into the area of high diffraction efficiency. The theory predicts efficiencies which in certain cases approach 100%, implying nearly total depletion of the irradiating wave.

H. Kogelnik applied the coupled wave theory to the problem of diffraction from volume holograms. This extensive analysis gives closed-form results for the angular and wavelength sensitivities for all possible hologram types. The coupled-wave theory assumes that there are only two waves present in the grating: the reference wave R and the diffracted signal wave S. It is assumed that the Bragg condition is approximately satisfied by these two waves and all other orders strongly violate the Bragg condition and hence are not present.

In Fig. 3, the grating assumed by Kogelnik for his analysis is shown.

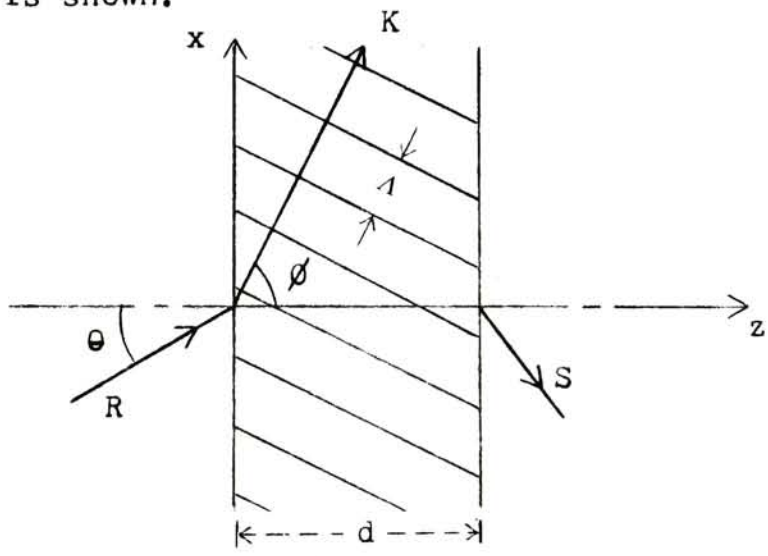

Fig. 3. Notation used to define a thick grating.

The z-axis is perpendicular to the surfaces of the medium, the x-axis is in the plane of incidence and parallel to the medium boundaries, and the y-axis is perpendicular to the page. The fringes are oriented perpendicular to the plane of incidence and slanted with respect to the medium boundaries at an angle of Θ. The grating vector $\vec{K}$ is oriented perpendicular to the fringes and is of length $K = 2\pi/\Lambda$, where Λ is the fringe spacing or the period of the grating. The angle of incidence of the irradiating wave R at the medium is Θ.

Wave propagation in the grating is described by the scalar wave equation

$$\nabla^2 \mathcal{E} + k^2 \mathcal{E} = 0 \tag{4}$$

where $\mathcal{E}(x,z)$ is the complex amplitude of the y-component of the electric field which is assumed to independent of y and to oscilate with angular frequency ω. $k(x,z)$ is the propagation constant. It is spatially modulated and related to the relative dielectric constant $\epsilon(x,z)$ and the conductivity $\sigma(x,z)$ of the medium by Equ. (5).

$$k^2 = \frac{\omega^2}{c^2} \epsilon - j\omega u \sigma \tag{5}$$

Where c is the speed of light in free space and μ is the permeability of the medium which is assumed to be equal to that of free space. The fringes of the hologram grating are represented by a spatial modulation of ϵ or σ in Equ. (6).

$$\epsilon = \epsilon_o + \epsilon_1 \cos(\vec{K}\cdot\vec{X})$$
$$\sigma = \sigma_o + \sigma_1 \cos(\vec{K}\cdot\vec{X}) \qquad (6)$$

Where ϵ_1 and σ_1 are the amplitudes of the spatial modulation, ϵ_o is the average dielectric constant, and σ_o is the average conductivity. ϵ and σ are assumed to be modulated in phase. The radius vector $\vec{X}$ and the grating vector $\vec{K}$ are defined by Equ. (7).

$$\vec{X} = \begin{pmatrix} x \\ y \\ z \end{pmatrix}; \qquad \vec{K} = K \begin{pmatrix} \sin\phi \\ 0 \\ \cos\phi \end{pmatrix}; \qquad K = 2\pi/\Lambda . \qquad (7)$$

Equ. (5) and (6) can be combined to give

$$k^2 = \frac{\omega^2}{c^2}[\epsilon_o + \tfrac{1}{2}\epsilon_1(e^{j\vec{K}\cdot\vec{X}} + e^{-j\vec{K}\cdot\vec{X}})] - j\omega\mu[\sigma_o + \tfrac{1}{2}\sigma_1(e^{j\vec{K}\cdot\vec{X}} + e^{-j\vec{K}\cdot\vec{X}})]$$

$$= \frac{\omega^2}{c^2}\epsilon_o - j\omega\mu\sigma_o + \left(\frac{\omega^2\epsilon_1}{2c^2} - \frac{j\omega\mu\sigma_1}{2}\right)(e^{j\vec{K}\cdot\vec{X}} + e^{-j\vec{K}\cdot\vec{X}}).$$

For the average propagation constant β and the average absorption constant α given by

$$\beta = \frac{2\pi(\epsilon_o)^{\frac{1}{2}}}{\lambda} \qquad \text{and} \qquad \alpha = \frac{\mu c\,\sigma_o}{2(\epsilon_o)^{\frac{1}{2}}},$$

the propagation constant becomes

$$k^2 = \beta^2 - 2j\beta\alpha + \left[\frac{\beta^2\epsilon_1}{\epsilon_o^{\frac{1}{2}}\,2} - \frac{j\beta\mu\sigma_1}{\epsilon_o^{\frac{1}{2}}}\right](e^{j\vec{K}\cdot\vec{X}} + e^{-j\vec{K}\cdot\vec{X}})$$

$$k^2 = \beta^2 - 2j\beta\alpha + 2\kappa\beta(e^{j\vec{K}\cdot\vec{X}} + e^{-j\vec{K}\cdot\vec{X}}) \qquad (8)$$

where κ is the coupling constant given by Equ. (9).

$$\kappa = \tfrac{1}{4}\left(\frac{2\pi\epsilon_1}{\epsilon_o^{\frac{1}{2}}} - \frac{j\mu c\sigma_1}{\epsilon_o^{\frac{1}{2}}}\right) \qquad (9)$$

This coupling constant describes the coupling between the reference and signal waves. It is the central parameter of the couple-wave theory.

Optical media are usually characterized by their refractive index and their absorption constant. If the following conditions are met

$$2\pi n/\lambda \gg \alpha \quad ; \quad 2\pi n/\lambda \gg \alpha_1 \quad , \quad n \gg n_1 \quad , \tag{10}$$

which is true in almost every case. Here n is the average refractive index, and n_1 and α_1 are the amplitudes of the spatial modulation of the refractive index and the absorption constant respectively. The average propagation constant then becomes

$$\beta = 2\pi n/\lambda \tag{11}$$

and the coupling constant is given by

$$\kappa = \pi n_1/\lambda - j\,\alpha_1/2 \; . \tag{12}$$

The total electric field in the grating is the superposition of the reference wave R and the signal wave S. In complex form this is given by Equ. (13).

$$\mathcal{E} = R(z)\, e^{-j\vec{\rho}\cdot\vec{X}} + S(z)\, e^{-j\vec{\delta}\cdot\vec{X}} \tag{13}$$

where ρ and δ are the propagation vectors which contain the information about the propagation constants and the direction of the propagation for the reference wave R and the signal wave S. Fig. 4 shows the propagation vectors and their proper orientation with respect to the grating vector K.

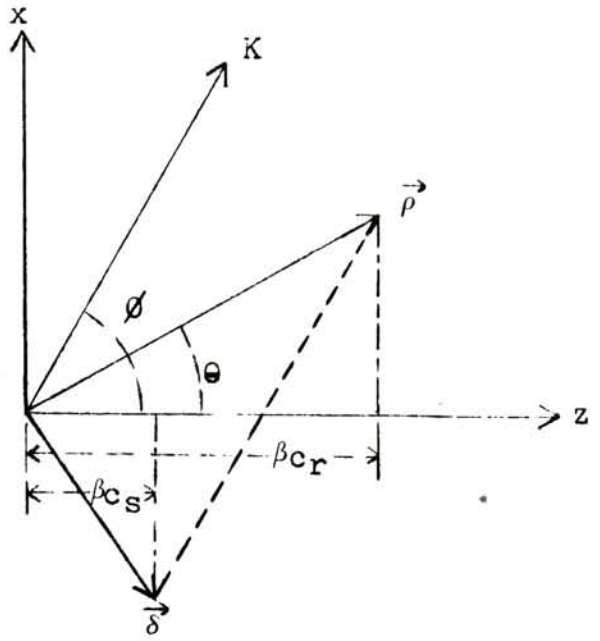

Fig. 4. The propagation vectors of the reference wave R and the signal wave S, $\vec{\rho}$ and $\vec{\delta}$, and their relation to the grating vector. The obliquity factors c_r and c_s are indicated.

The relation between the propagation vectors and the grating vector is given by Equ. (14).

$$\vec{\delta} = \vec{\rho} - \vec{K} \tag{14}$$

The components of $\vec{\rho}$ are given by Equ. (15).

$$\vec{\rho} = \begin{pmatrix} \rho_x \\ 0 \\ \rho_z \end{pmatrix} = \beta \begin{pmatrix} \sin \Theta \\ 0 \\ \cos \Theta \end{pmatrix} \tag{15}$$

From Equ. (15) and Equ. (14), the components of $\vec{\delta}$ are found to be

$$\vec{\delta} = \begin{pmatrix} \delta_x \\ 0 \\ \delta_z \end{pmatrix} = \beta \begin{pmatrix} \sin \Theta - \frac{\vec{K}}{\beta} \sin \emptyset \\ 0 \\ \cos \Theta - \frac{\vec{K}}{\beta} \cos \emptyset \end{pmatrix} . \tag{16}$$

The vector relation in Equ. (14) is shown in Fig. 5 together with a circle of radius K . The general case is shown in Fig. 5a, where the Bragg condition is not satisfied and the length of δ differs from β . Fig. 5b shows the same diagram for the incidence at the Bragg angle Θ_o. In this special case the lengths of both δ and ρ are equal to the free propagation constant β , and the Bragg condition is obeyed and is given by Equ. (17).

$$\cos (\phi - \Theta) = K/2\beta \qquad (17)$$

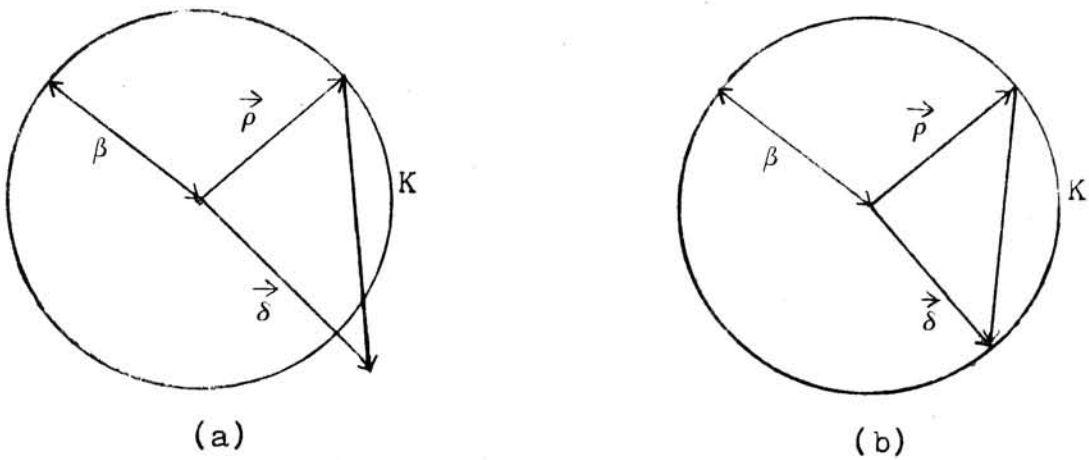

Fig. 5. Vector diagram (conservation of momentum) for (a) near and (b) exact Bragg incidence.

To obtain the coupled-wave equations, combine Equs. (4) and (8) and insert the expressions (13) and (14). Then compare the terms with equal exponentials. This derivation can be found in appendix A with the result that the coupled-wave equations can be written in the form of Equs. (18) and (19).

$$c_r R' + R = -j\kappa S \tag{18}$$

$$c_s S' + (\alpha + j\Theta)S = -j\kappa R \tag{19}$$

Where c_s and c_r are the obliquity factors given by Equ. (20).

$$\begin{aligned} c_s &= \rho_z/\beta = \cos\Theta \\ c_r &= \delta_z/\beta = \cos\Theta - \frac{K}{\beta}\cos\phi \end{aligned} \tag{20}$$

Also a dephasing measure is introduced. This is a factor which allows for deviations in the angle of incidence and correct wavelength. It is given by Equ. (21).

$$\Theta = (\beta^2 - \delta^2) / 2\beta \tag{21}$$

The energy balance of the coupled-wave model is obtained by multiplying Equs. (18) and (19) by R* and S*, the complex conjugates of the reference and signal waves respectively, and then adding. This is given by Equ. (22).

$$(c_r RR^* + c_s SS^*)' + 2(RR^* + SS^*) + j(\kappa - \kappa^*)(RS^* + R^*S) = 0 \tag{22}$$

The general solution of the coupled-wave equations is given by Equs. (23) and (24).

$$R(z) = r_1 e^{\gamma_1 z} + r_2 e^{\gamma_1 z} \tag{23}$$

$$S(z) = s_1 e^{\gamma_1 z} + s_2 e^{\gamma_2 z} \tag{24}$$

Where r_i and s_i $(i = 1,2)$ are constants which depend on the boundary conditions and γ_i are constants which are derived in appendix B with the result given by Equ. (25).

$$\gamma_{1,2} = -\tfrac{1}{2}\left(\frac{\alpha}{c_r} + \frac{\alpha}{c_s} + \frac{j\Theta}{c_s}\right) \pm \tfrac{1}{2}\left(\left(\frac{\alpha}{c_r} - \frac{\alpha}{c_s} - \frac{j\Theta}{c_s}\right)^2 - \frac{4\kappa^2}{c_r c_s}\right)^{\frac{1}{2}} \tag{25}$$

The boundary conditions for transmission holograms are given by Equ. (26) where $c_s > 0$.

$$R(0) = 1 , \qquad S(0) = 0 \tag{26}$$

If these boundary conditions are inserted into Equs. (23) and

(24), it follows that

$$r_1 + r_2 = 1 \quad \text{and} \quad s_1 + s_2 = 0 \tag{27}$$

If, Equs. (23) and (24) are inserted into Equ. (19) and Equ. (27) is applied, then the result is given by Equ. (28).

$$s_1 = -s_2 = -j\kappa / c_s \, (\gamma_1 - \gamma_2) \tag{28}$$

Introducing these constants in Equ. (24), the expression for the amplitude of the signal wave at the output of the grating is given by Equ. (29).

$$S(d) = j \frac{\kappa}{c_s(\gamma_1 - \gamma_2)} (e^{\gamma_2 d} - e^{\gamma_1 d}) \tag{29}$$

Where d is the thickness of the grating.

The diffraction efficiency for transmission holograms is given by Equ. (30).

$$\eta = \frac{|c_s|}{|c_r|} SS^* \tag{30}$$

Where η is the fraction of the incident light power which is diffracted into the signal wave, and S is the complex amplitude of the output signal for a reference wave R incident with unit amplitude.

For transmission holograms, we recall that c_s is positive and the output signal appears at z = d. Combining Equs. (25) and (29) leads to the general formula for the amplitude of the signal S which is given by Equ. (31).

$$S = \frac{-j(c_r/c_s)^{\frac{1}{2}}\, e^{(-\alpha d/c_r)}\, e^{\xi} \sin(\nu^2 - \xi^2)^{\frac{1}{2}}}{(1 - \xi^2/\nu^2)^{\frac{1}{2}}}$$

$$\nu = \kappa d/(c_r c_s)^{\frac{1}{2}} \qquad (31)$$

$$\xi = \tfrac{1}{2} d \left(\frac{\alpha}{c_r} - \frac{\alpha}{c_s} - \frac{j\Theta}{c_s}\right)$$

The derivation of Equ. (31) can be found in the appendix.

If the hologram is considered to be a lossless dielectric grating, then the coupling constant $\kappa = \pi n_1/\lambda$ and the absorption constant $\alpha = \alpha_1 = 0$. Equ. (31) can then be re-written in the form given by Equ. (32).

$$S = \frac{-j(c_r/c_s)^{\frac{1}{2}}\, e^{-j} \sin(\nu^2 + \xi^2)^{\frac{1}{2}}}{(1 + \nu^2/\xi^2)^{\frac{1}{2}}}$$

$$\nu = \pi n_1 d/(c_r c_s)^{\frac{1}{2}} \qquad (32)$$

$$\xi = \Theta d/2c_s$$

The associated formula for the diffraction efficiency is given by Equ. (33)

$$\eta = \frac{\sin^2(\nu^2 + \xi^2)}{(1 + \xi^2/\nu^2)} \qquad (33)$$

If there is no slant ($\phi = \pi/2$) and if the Bragg condition is obeyed then $c_r = c_s = \cos\theta$ and Equ. (33) is reduced to Equ. (34).

$$\eta = \sin^2(\pi n_1 d/\lambda \cos\theta_o)$$

$$= \tfrac{1}{2} - \tfrac{1}{2}\cos(2\pi n_1 d/\lambda \cos\theta_o) \qquad (34)$$

This equation implies that a hologram, which has a thickness d, an amplitude of the spatial modulation of the refractive index n_1, and a construction wavelength λ, is capable of

100% diffraction efficiency at specific Bragg angles. This is plotted in Fig. 6 for some typical values of d, n_1, and λ.

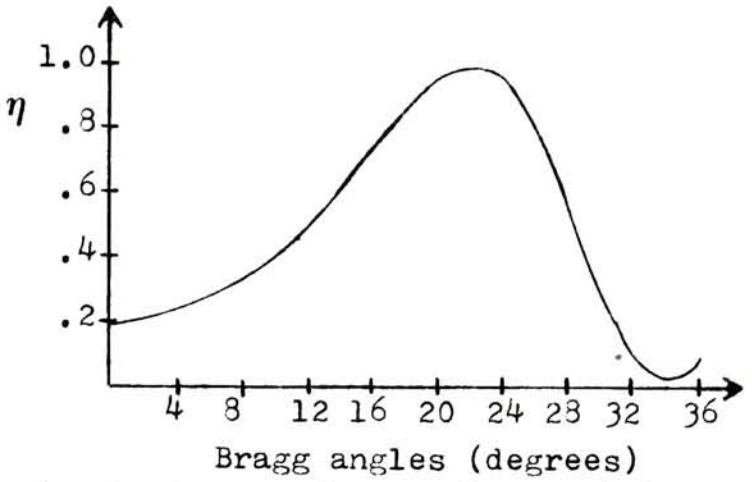

Fig. 6. A plot of diffraction efficiency as a function of Bragg angle for d = 7μm, n_1 = .37, and λ = .6328μm.

Transmission holograms have imaging characteristics[6] which make it possible to obtain either real images or virtual images. The construction geometry required to construct a hologram of a point source is shown in Fig. 7.

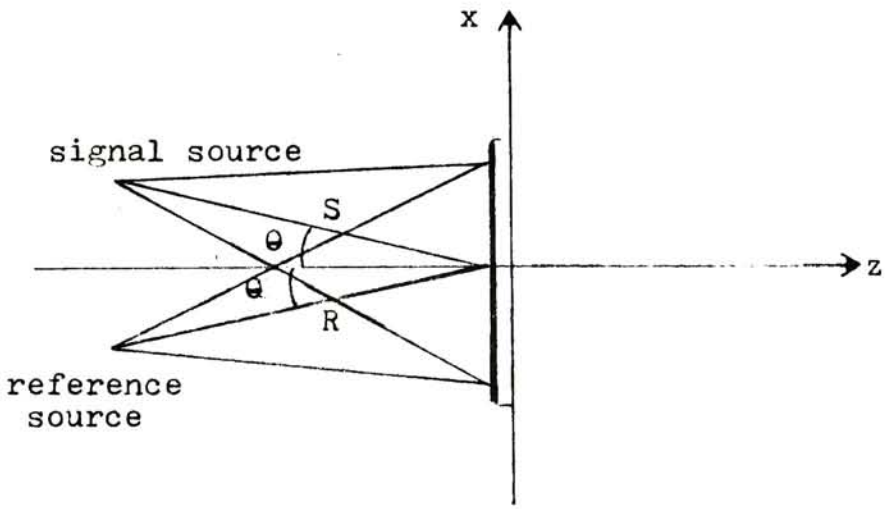

Fig. 7. Construction geometry for a hologram of a point source.

Where θ and R are the reference wave angle and radius respectively, and θ and S are the signal wave angle and radius respectively. If the hologram, constructed with the geometry shown in Fig. 7, is irradiated with the reference wave used in construction, then a virtual image of the signal source is seen from the right side looking left into the hologram. This is shown in Fig. 8.

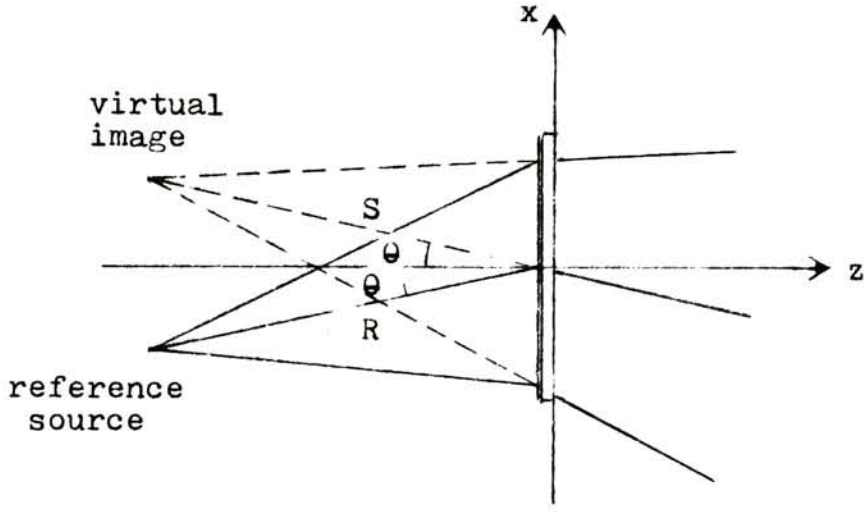

Fig. 8. Reconstruction geometry for a virtual image.

If the hologram is irradiated with a reference wave which is conjugate to the reference wave used in construction, then the image created by this geometry is a real conjugate image. This is shown in Fig. 9.

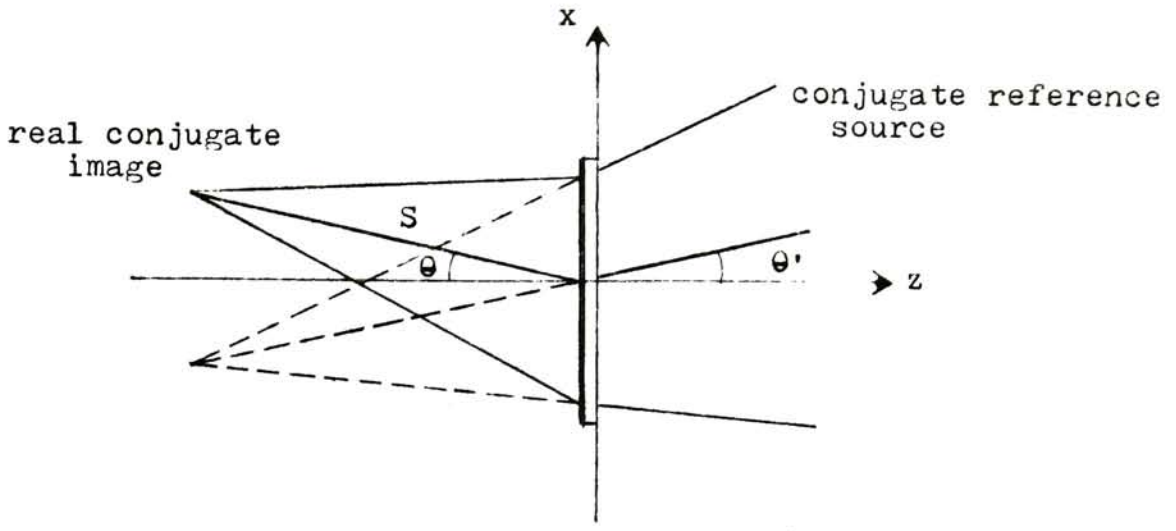

Fig. 9. Reconstruction geometry for a real image.

A real conjugate image is characterized by a depth inversion. If our signals are two-dimensional, then this depth inversion will have no effect on the resultant real image. It is the latter imaging characteristic which makes it possible for a hologram to focus light into any pattern. By putting enough energy into this focal pattern, a laser machining operation can be performed.

In Moran's experiments, a holographic lens for laser machining was constructed in a dichromated gelatin (DCG). The DCG can form a volume, phase hologram with high diffraction efficiency that can withstand high energy densities due to its low absorption. But the spectral sensitivity of the DCG only extends out to 550nm. This made it necessary to construct the holographic lens at the 488.0nm line of the argon laser. When machining was performed with the 649.3nm line of the ruby laser, the holographic lens had to be shifted

away from Bragg's angle due to the wavelength difference. This gave a corresponding decrease in the diffraction efficiency.

In Schwartz's work, he hoped to solve the problem due to the difference in wavelength by producing the holographic lens at the 632.8nm line of the He-Ne laser. To do this he first made an absorption hologram on a panchromatic emulsion and then contact printed this onto the DCG to produce the high efficiency hologram. This would give a holographic lens at wavelengths closer to those used for laser machining with a ruby laser. This method did not prove feasible due to problems with replication.

This research has also approached the problem due to the difference in reconstruction wavelength by constructing the holographic lens at the 632.8nm line of the He-Ne laser. But instead of the ineffective replication procedure Schwartz used, high efficiency, low absorption holographic lenses are produced directly by bleaching panchromatic silver halide emulsions.

EXPERIMENTAL

Initially this experiment was concerned with the construction of the simplest type of holographic lens. This lens has a single focal point and is constructed by making a hologram of a point source. A photograph of the apparatus which gave the optimum image quality is shown in Fig. 10 and schematically represented in Fig. 11. The optical table is insulated from vibrations by placing it on two partially air filled inner-tubes. It can be seen in Fig. 11 that the signal wave angle is chosen to be Brewster's angle (56.7^{o} for glass) and the reference wave angle is zero. If the construction light is polarized parallel to the table, this construction geometry is an effective method of reducing reflection images. These images are caused by relections of the construction waves off the rear surface of the glass plate. The irradiance of the reference wave was .062mJ/cm^2. And the irradiance of the signal wave was .034mJ/cm^2. Four exposures were placed on a 4" x 5" Kodak type 649F spectroscopic plate which was reversal bleached processed[7] to give a phase hologram. The procedure for this process is given in Table 1.

Fig. 10. Photograph of the apparatus used to construct a single focal point holographic lens

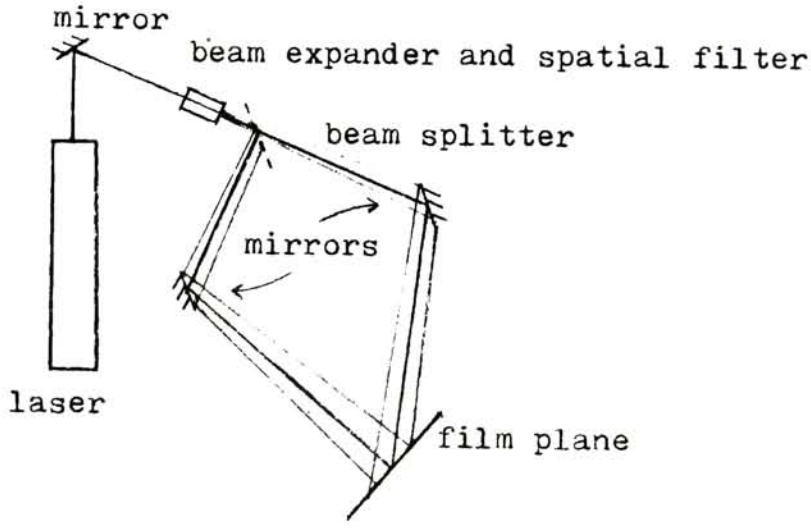

Fig. 11. Schematic representation of the apparatus in Fig. 10.

TABLE 1

1.	Kodak Special Developer SD-48	8 min.
2.	Kodak Stop Bath SB-1	15 sec.
3.	Rinse in running water	1 min.
4.	Kodak Bleach Bath R-9	2 min.
5.	Rinse in running water	3 min.
6.	Kodak Stain Remover S-13 part A	1 min.
7.	Kodak Stain Remover S-13 part B	1 min.
8.	Rinse in running water	5 min.
9.	Rinse in methanol diluted 1:1 with water	1 min.
10.	Rinse in methanol	30 sec.
11.	Repeat 10 with fresh methanol	30 sec.
12.	Dry rapidly with forced air	

all solutions are 75°F

To evaluate the holographic lenses, the real image of the point source is reconstructed. A photograph of the apparatus is shown in Fig. 12 and schematically represented in Fig. 13. As can be seen the conjugate reference wave is created with a spherical lens. The diffraction efficiency of the holographic lens is determined by taking the ratio of the flux incident on the lens to the flux diffracted into the image. The image quality is evaluated by recording the real image on film and scanning this on a microdensitometer.

Later it became desirable to make a holographic lens which has a focal pattern instead of a focal point. A photograph of the apparatus is shown in Fig. 14 and schematically represented in Fig. 15. The focal pattern for this lens is shown in Fig. 15a.

Fig. 12. Photograph of the apparatus used to reconstruct the real image.

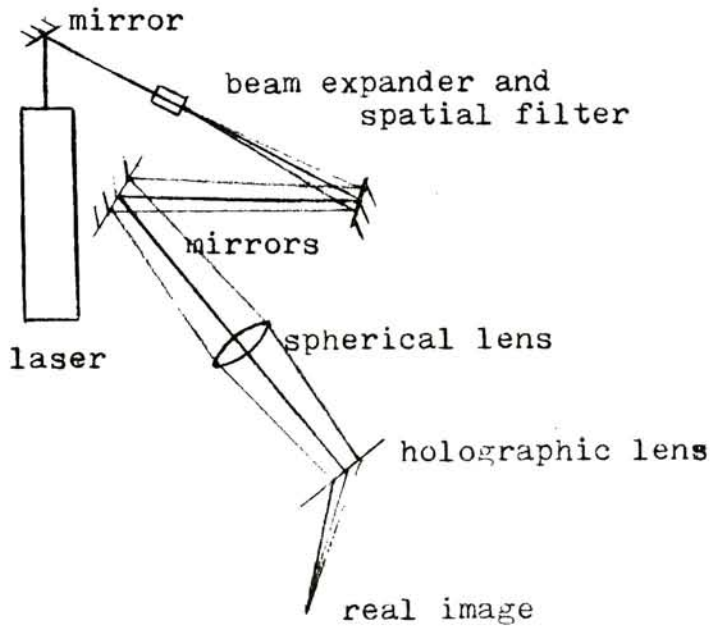

Fig. 13. Schematic representation of the apparatus in Fig. 12.

Fig. 14. Photograph of the apparatus used to construct the holographic lens which focuses into a pattern.

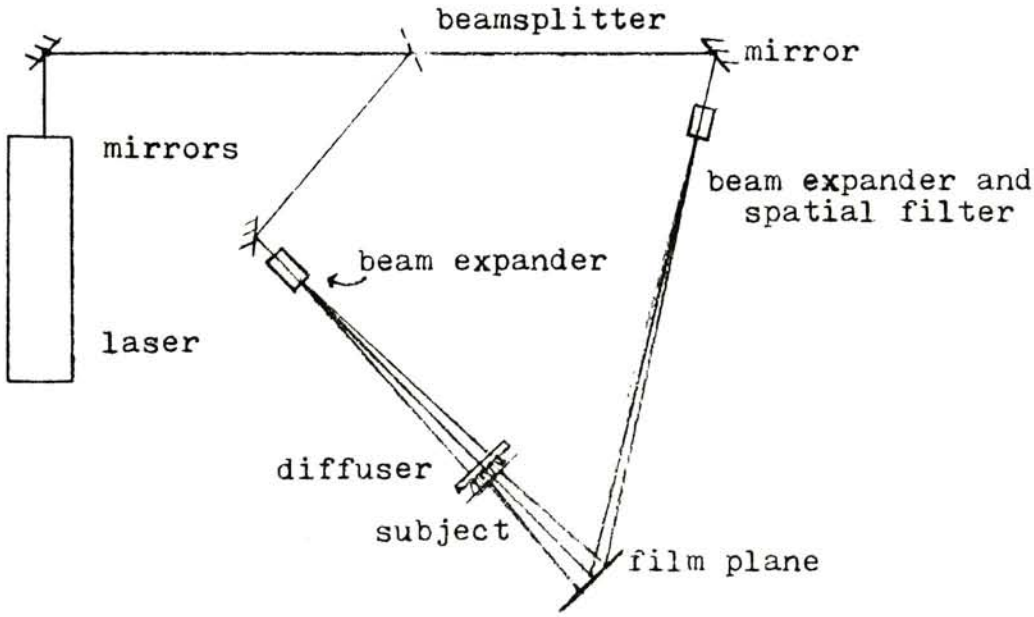

Fig. 15. Schematic representation of the apparatus in Fig. 14.

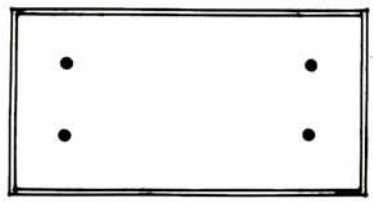

Fig. 15a. Lens focal pattern.

This pattern is copied on lith film at a four times reduction, and is meant to give a graphical example of how well the system works. The lith negative is back-lit with diffuse laser irradiation as shown in Fig. 14. This construction geometry is basically the same as that used for the single focal point holographic lens. The difference is the signal wave and reference wave are reversed.

The exposures are made on 4" x 5" Agfa type 8E75 Scientia plates with a beam ratio of approximately one to one. The process is as described in Table 1 with the exception that the plate was presoaked[3] in Kodak Prehardener SH-5 for 10 minutes and the development was correspondingly doubled. To determine the repeatability of the process and get a more precise relationship between diffraction efficiency and exposure, 16 exposures are placed on 4 plates. These

exposures ranged from $30\mu J/cm^2$ to $230\mu J/cm^2$.

These holographic lenses are evaluated as described previously for the single focal point holographic lenses. The reconstruction apparatus is basically the same as shown in Fig. 12 and schematically represented in Fig. 13. The only difference is the reference wave angle. The method of determining the diffraction efficiency and the image quality is also the same.

RESULTS

In the first part of this thesis, a holographic lens is produced by making a hologram of a point source on Kodak type 649F spectroscopic plates. These plates were exposed and then processed according to Table 1. The diffraction efficiency as a function of exposure is plotted in Fig. 16.

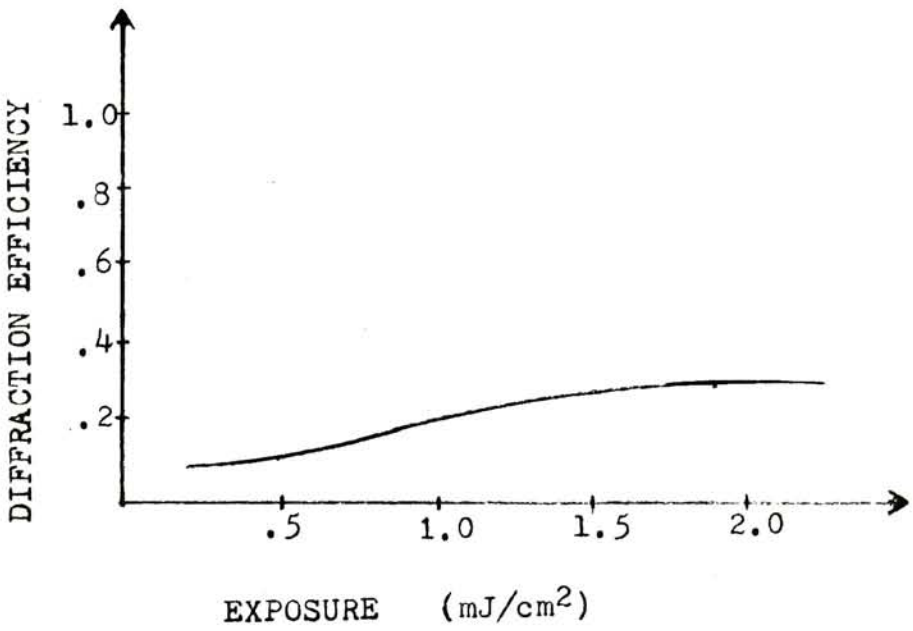

Fig. 16. Diffraction efficiency as a function of exposure.

The image quality of the lens is evaluated by recording the real image of the hologram on Kodak type Royal Pan film. A ten times enlargement of this record of the real image is shown in Fig. 17.

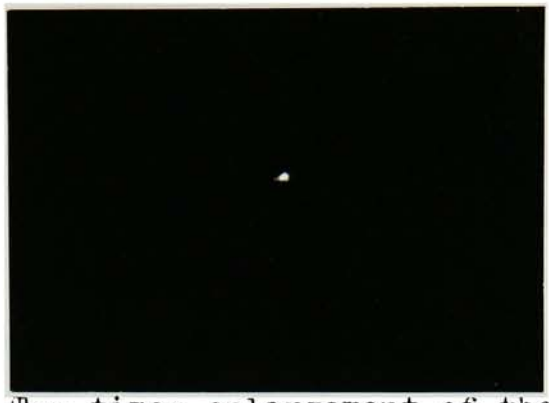

Fig. 17. Ten times enlargement of the lens's focal point.

This image should be a hard spot. The degradation could be attributed to the difficulty experienced in producing the exact conjugate reference wave. A more sophisticated apparatus would have solved this problem. A microdensitometer scan of the real image is shown in Fig. 18.

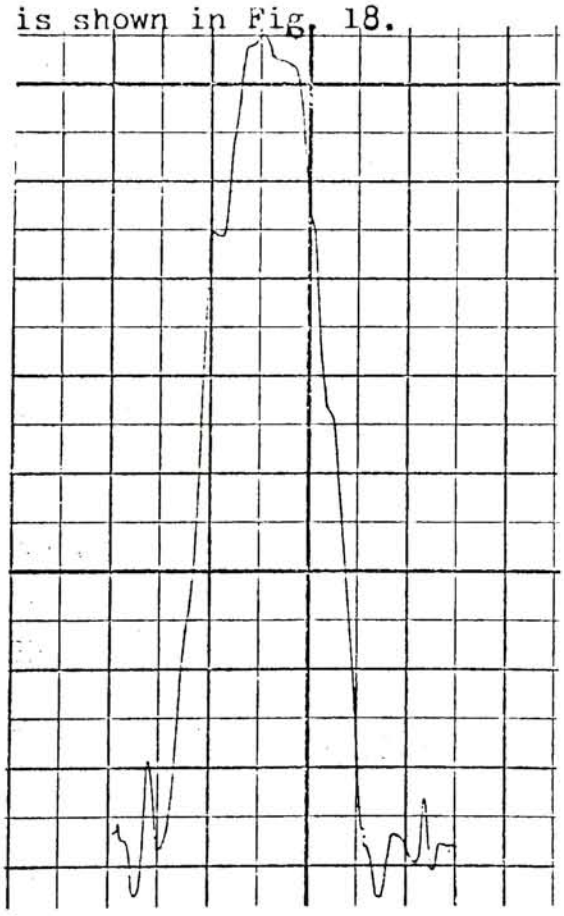

Fig. 18. Microdensitometer scan of the real image for a single focal point holographic lens.

This scan is made across the image at its smallest diameter. From this scan, which is about .9" wide, the image width can be calculated. The image is scanned with a 10μm circular aperature at a speed of .25mm/min. The chart recorder has a speed of 2"/min. This indicates that the image is approximately 100μm wide.

The holographic lens, which focuses into the pattern shown in Fig. 15a, is constructed on Agfa type 8E75 Scientia plates. The process for these plates is given in Table 1 with the exception that the plate is presoaked in a prehardener for 10 minutes and the development is doubled. Sixteen exposures are made on 4 - 4" x 5" plates which ranged from 30μJ/cm^2 to 230μJ/cm^2. Each plate is processed separately to determine the repeatability of the process. One plate and two exposures had to be eliminated due to visible physical defects in the plates which can be attributed to the age of the plates. The diffraction efficiency as a function of exposure is shown in Fig. 19.

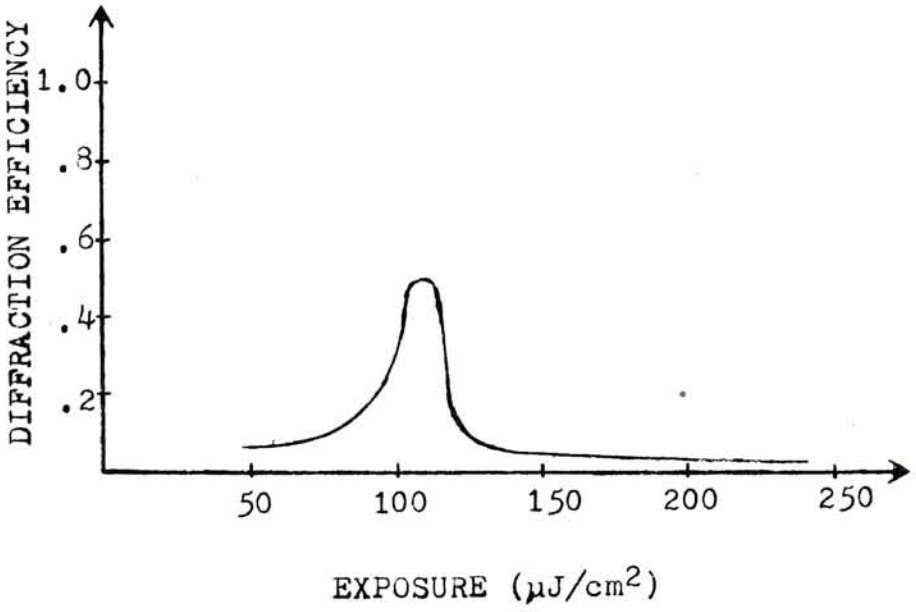

Fig. 19. Diffraction efficiency as a function of exposure for the holographic lens that has a focal pattern.

The image quality of these lenses is evaluated as before. The real image of the hologram is recorded on Kodak type Royal Pan film. An enlargement of this real image is shown in Fig. 20.

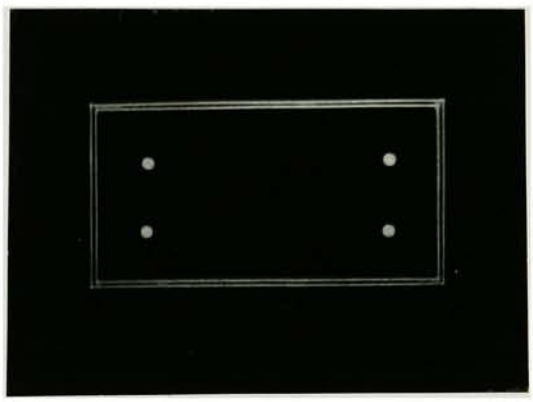

Fig. 20. An enlargement of the real image for a holographic lens that has a focal pattern.

The quality of this image is also highly dependent on the alignment of the holographic with the exact conjugate reference wave. A microdensitometer scan, of the line pair where good reconstruction is obtained, is shown in Fig. 21. The scanning aperture is 10μm and the scan rate is .25mm/min. The chart recorder speed is 2"/min.

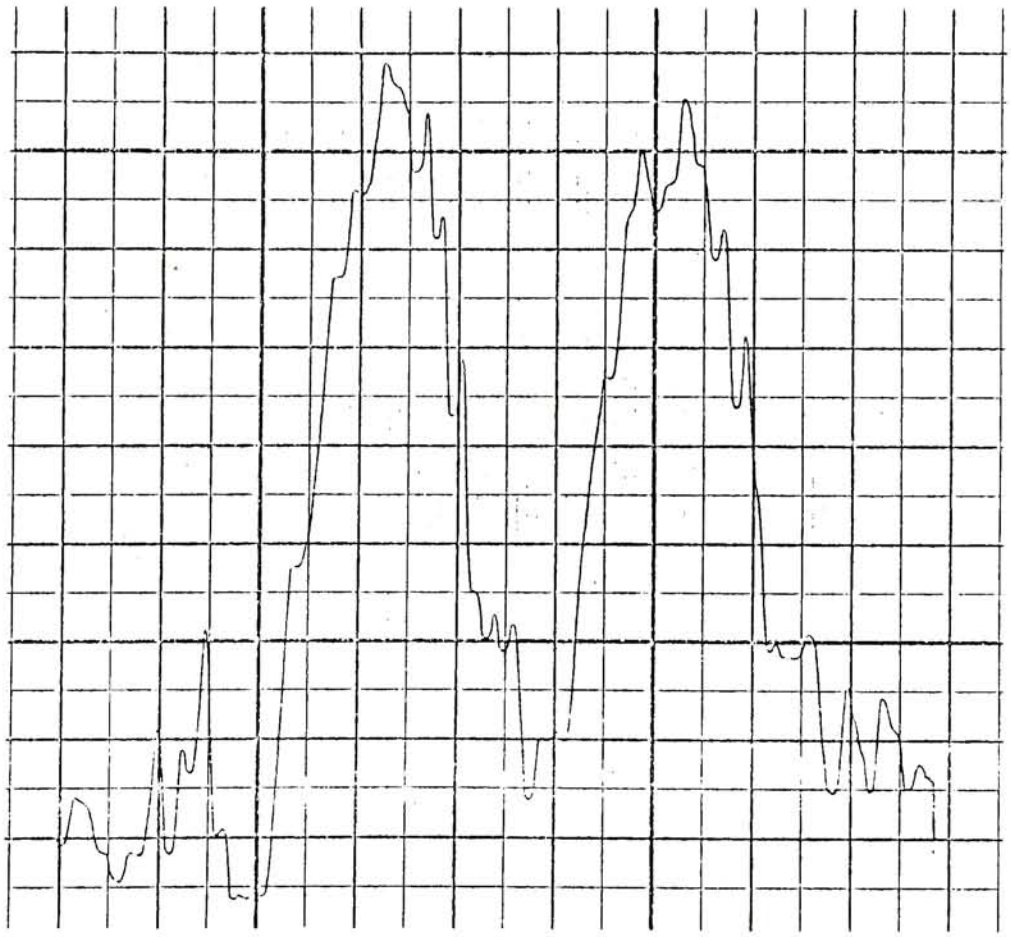

Fig. 21. Microdensitometer scan of a line pair from the real image of a holographic lens with a focal pattern.

DISCUSSION

The primary objective of this thesis was to obtain a higher diffraction efficiency holographic lens at wavelengths closer to those used for laser machining. This was accomplished by bleaching panchromatic photographic emulsions. It can be seen in Fig. 16 that 32% diffraction efficiency at a $2mJ/cm^2$ exposure was obtained with holographic lenses that have a single focal point. These lenses were constructed on Kodak type 649F spectroscopic plates that were reversal bleach processed according to Table 1. This maximum diffraction efficiency was not as high as some of the lenses produced in the first screening experiments. This geometry creates fringes that are slanted at an angle of 28.35° which, along with the three to one beam ratio, could account for the lower diffraction efficiency. In the screening experiments, lenses were produced with no slant and one to one beam ratio which had 40% diffraction efficiency. This is the maximum efficiency as claimed by the literature[7] for this film-process combination. The image quality, which is shown in Fig. 17, is not as high as the literature indicates possible[2]. It could be increased if better equipment were used in an environment which had more control over sound, air currents, mechanical stability, and dust in the air. The image degradation could also be improved with less exposure on the film. In addition, it is difficult to gauge how well a lens

would on a laser machining operation compared to how well it images on film.

In the production of the single focal point lenses there was some concern for reflection images. These images were caused by the reflection of the construction waves off the rear surface of the plate. The power in these images was only 3% of the power in the primary image. This is probably not enough power to affect the quality of the laser machining, but it was found that the construction geometry shown in Fig. 11 could almost totally eliminate these reflection images.

After producing a holographic lens of higher diffraction efficiency, it became desirable to devise a method of producing a holographic lens which could focus into a pattern. For this a graphical pattern, shown in Fig. 15a, was chosen to evaluate the imaging quality of the system. This lens would not be practical for laser machining due to its large surface area. For this holographic lens, Agfa type 8E75 Scientia plates were used. R. Lamberts, of Kodak Research Labs, suggested that, if these plates were to be reversal bleach processed according to Table 1, they should be presoaked in a pre-hardener.

It can be seen in Fig. 19, that the maximum diffraction efficiency was 50% for this film-process combination. It should be noted that there was some unwanted diffraction outside the image which is not shown in Fig. 20. This

unwanted diffraction showed up in the form of soft lines which were horizontal to the image and located above and below the image. This unwanted diffraction was caused by a low frequency (250 C / mm) diffraction pattern on the hologram. This low frequency pattern was probably caused by diffraction of residual undiffused laser irradiation off the edges of the subject. This unwanted diffraction could possibly be reduced with a better method of diffusing the laser light. If it couldn't be reduced then it would result in a reduction (approx. 5%) in the usable diffraction efficiency and would not effect the quality of the laser machining.

The resulting image quality can be seen in Fig. 20. This image could also be improved with a more sophisticated apparatus.

A typical laser machining application for the holographic lens might be to drill 4 holes in a circuit board or piece of metal. For laser machining, power densities, 250KW/cm^2 to 50MW/cm^2, are needed to do laser metalworking.[9] If each hole is 100μm in diameter, then the total area of the focal pattern is approximately 8×10^{-5} cm^2. To obtain power densities of 50MW/cm^2, then about 4KW would have to be focused into the pattern. If the lens has a diffraction efficiency of 45%, then a 9KW laser should be sufficient to drill the holes. This would be a relatively low-power ruby laser. Today ruby lasers are available which can produce as much as 10^9 watts. These high-power lasers could conceivably do

a laser machining operation over a much larger area. It should be noted that these very high-power lasers are correspondingly much more expensive and this has to be taken into account in the cost analysis of the desired machining operation.

This thesis also investigated another film-process combination. The film was Kodak type 131-02 highspeed holographic plates, and the process was to produce a high density absorption hologram which is bleached with dry bromine vapor. The diffraction efficiency for this film-process combination was a 40% maximum. More information on this can be found in Appendix D.

Since the proposal of this project, two other processes[10,11] were discovered to give high efficiency holographic optical elements (HOE) at wavelengths closer to those used for laser machining. The first process involves Kodak type 120-02 holographic plates which are developed to produce a high density absorption hologram which is subsequently bleached with dry bromine vapor. The second process involves spectrally sensitizing dichromated gelatin emulsions out to the wavelength of the He-Ne laser. The dry bleach process in conjunction with the type 120 plates is capable of diffraction efficiencies as high as 70%. The spectrally sensitized emulsions are capable of 80% diffraction efficiency but require much larger exposures. Both of these film-process combinations should be investigated for this application of HOE's.

What remains to be done with research is to find a company which has the resources and the funds to apply these HOE's to laser machining operations. This is a key step in determining the real feasibility of this idea.

LIST OF REFERENCES

1. Kogelnik, H., "Coupled Wave Theory for Thick Hologram Gratings", The Bell System Technical Journal, Nov. 1969, v. 48, p. 2909.

2. Moran, J. M., "Laser Machining with a Holographic Lens", Applied Optics, v. 18, p. 412, (1971).

3. Schwartz, E., "Laser Imaging with a Holographically Produced Lens", senior research thesis at R.I.T., 1977.

4. Collier, Burckhardt, Lin, Optical Holography, Academic Press, New York, 1971.

5. Bragg, W.L., "The Diffraction of Short Electromagnetic Waves by a Crystal", Proc. Cambride Phil. Soc. 17, 43, (1912).

6. Smith, H. M., Principles of Holography, John Wiley & Sons, New York, 1975, p. 109.

7. Lamberts, R. L. and Kurtz, C. N., "Reversal Bleaching for Low Flare Light in Holograms", Applied Optics, v. 10, p. 1342, (1971).

8. Lamberts, R. L. personal communication (3/78).

9. Goldman, L., Applications of the Laser, CRC Press, Cleveland, Ohio, 1973, p. 50.

10. Graube, A., "Advances in Bleaching Methods for Photographically Recorded Holograms", Applied Optics, v. 13, p. 2942, (1974).

11. Graube, A., "Dye-Sensitized Dichromated Gelatin for Holographic Optical Element Fabrication", P. S. & E., v. 22, no. 1, p. 37, (1978).

APPENDICES

APPENDIX A

Derivation of the coupled-wave equations

Apply the electric field, Equ. 13, and the propagation constant, Equ. 8, to the scalar wave equation, Equ. 4.

$$\varepsilon = R(z)e^{-j\rho\cdot x} + s(z)e^{-j\delta\cdot x} \tag{13}$$

$$k^2 = \beta^2 - 2j\beta\alpha + 2\kappa\beta(e^{jK\cdot X} + e^{-jK\cdot X}) \tag{8}$$

$$\nabla^2\varepsilon + k^2\varepsilon = 0 \tag{4}$$

$$\nabla^2(R(z)e^{-j\rho\cdot X} + S(z)e^{-j\delta\cdot X}) + \beta^2 - 2j\beta\alpha + 2\kappa\beta(e^{jK\cdot X} + e^{-jK\cdot X})$$
$$(R(z)e^{-j\rho\cdot X} + S(z)e^{-j\delta\cdot X}) = 0$$

$$e^{-j\rho\cdot X}(R'' - 2j\rho_z R' - 2j\beta\alpha) + e^{-j\delta\cdot X}(S'' - 2j\delta_z S' - (2j\beta\alpha + (\beta^2-\delta^2))S)$$
$$+ 2\kappa\beta R(e^{-j(\rho-K)\cdot X} + e^{-j(\delta+K)\cdot X})$$
$$+ S(e^{-j(\rho-K)\cdot X} + e^{-j(\delta+K)\cdot X}) = 0$$

Then compare the terms with equal exponentials ($e^{-j\rho\cdot X}$ and $e^{-j\delta\cdot X}$) apply Equ. (14) and neglect the waves in the $\rho + K$ and $\delta - K$ direction.

$$\delta = \rho - K \tag{14}$$

$$R'' - 2j\rho_z R' - 2j\alpha\beta R + 2\kappa\beta S = 0$$

$$S'' - 2j\delta_z S' - 2j\alpha\beta S + (\beta^2 - \delta^2)S + 2\kappa\beta R = 0$$

Assume the energy interchange is slow and neglect R" and S". Then apply the obliquity factors, Equ. (20) and the dephasing measure, Equ. (21)

$$c_r = \rho_z/\beta \qquad c_s = \delta_z/\beta \tag{20}$$

$$\Theta = \frac{\beta^2 - \delta^2}{2\beta} \tag{21}$$

The result is the coupled-wave equations, Equs. (18) and (19).

$$c_r R' + \alpha R = -j\kappa S \tag{18}$$

$$c_s S' + (\alpha + j\Theta) S = -j\kappa R \tag{19}$$

APPENDIX B

Solution of the coupled-wave equations

The form of the general solution is given by Equs. (23) and (24).

$$R(z) = r_1 e^{\gamma_1 z} + r_2 e^{\gamma_2 z} \tag{23}$$

$$S(z) = s_1 e^{\gamma_1 z} + s_2 e^{\gamma_2 z} \tag{24}$$

To determine the constants γ and γ , insert Equs. (23) and (24) into the coupled-wave equations

$$(c_r \gamma_i + \alpha)\, r_i = -j\kappa s_i$$

$$(c_s \gamma_i + \alpha + j\Theta)\, s_i = -j\kappa r_i \qquad i = 1, 2$$

Then multiply these equations to obtain a quadratic equation for γ_i.

$$\gamma_i^2 + \left(\frac{\alpha}{c_s} + \frac{\alpha}{c_r} + j\frac{\Theta}{c_s}\right)\gamma_i + \frac{\alpha^2}{c_r c_s} + j\frac{\Theta d}{c_r c_s} + \frac{\kappa}{c_r c_s}^2 = 0$$

Then apply the quadratic formula.

$$\gamma_i = -\tfrac{1}{2}\left(\frac{\alpha}{c_s} + \frac{\alpha}{c_r} + j\frac{\Theta}{c_s}\right) \pm \tfrac{1}{2}\left(\left(\frac{\alpha}{c_r} - \frac{\alpha}{c_s} - j\frac{\Theta}{c_s}\right)^2 - 4\,\frac{\kappa^2}{c_r c_s}\right)^{\frac{1}{2}}$$

APPENDIX C

Derivation of the output signal for a transmission hologram

Apply the solution of the coupled-wave equations, Equ. (25), to the expression for the amplitude of the signal wave for a transmission hologram. Using the following relations

$$\nu = \kappa d/(c_r c_s)^{\frac{1}{2}}$$

and

$$\xi = \tfrac{1}{2} d \left(\frac{\alpha}{c_r} - \frac{\alpha}{c_s} - j\frac{\Theta}{c_s}\right)$$

the signal becomes

$$S(d) = -j \frac{(c_r c_s)^{\frac{1}{2}} \nu}{d c_s \left(\frac{4\xi^2}{d^2} - \frac{4\nu^2}{d^2}\right)^{\frac{1}{2}}} e^{\frac{d}{2}\left(\frac{\xi 2}{d} - \frac{2\alpha}{c_r}\right) + \frac{d}{2}\left(\frac{4\xi^2}{d^2} - \frac{4\nu^2}{d^2}\right)^{\frac{1}{2}}}$$

$$- e^{\frac{d}{2}\left(\frac{\xi 2}{d} - \frac{2\alpha}{c_r}\right) - \frac{d}{2}\left(\frac{4\xi^2}{d^2} - \frac{4\nu^2}{d^2}\right)^{\frac{1}{2}}}$$

$$= - \frac{(c_r c_s)^{\frac{1}{2}}}{2\left(1 - \frac{\xi^2}{\nu^2}\right)^{\frac{1}{2}}} e^{\xi} e^{-\left(\frac{\alpha d}{c_r}\right)} e^{j(\nu^2 - \xi^2)^{\frac{1}{2}}} - e^{-j(\nu^2 - \xi^2)^{\frac{1}{2}}}$$

$$= -j \frac{(c_r c_s)^{\frac{1}{2}}}{\left(1 - \frac{\xi^2}{\nu^2}\right)^{\frac{1}{2}}} e^{\xi} e^{-\left(\frac{\alpha d}{c_r}\right)} \sin(\nu^2 - \xi^2)^{\frac{1}{2}}$$

APPENDIX D

Additional information on Kodak type 131-02 high speed holographic plates

Another film-process combination was also investigated. This was Kodak high-speed holographic plates which were processed to a high density (3.0 - 4.0) absorption hologram. This hologram was then bleached with dry bromine vapor.

The processing procedure for producing the high density absorption hologram is given in Table 1D.

TABLE 1D

1.	Develop in D-19	5 min.
2.	Kodak Stop Bath SB-1	15 sec.
3.	Kodak F-5 Fixer	5 min.
4.	Wash	1 min.
5.	Hypo clear	4 min.
6.	Wash	3 min.
7.	Rinse (3 parts methanol, 1 part water)	5 min.
8.	Wash	5 min.
9.	Photo-flo	2 min.

all processing done at 68°F

In that liquid bromine is very dangerous to work with, all bleaching was done under the fume hood in the photo-chem lab. The absorption holograms were subjected to specific vapor concentrations of bromine. This was determined by the volume of the container for bleaching and the exposed surface area of liquid bromine. For 25 square centimeters of plate to be bleached in a 315 cubic centimeter container, ten square

centimeters of exposed liquid bromine are needed. In addition several ml's of hot water were placed in the bottom of the container. This raised the relative humidity in the container, and allowed the bromine to diffuse into the emulsion at a higher rate. Under these conditions it would take approximately one hour to convert the silver to silver bromide. After processing the plates appear yellow.

An exposure series was made using the same set-up described in the experimental section for making a holographic lens with a focal pattern. The density as a function of log exposure is plotted in Fig. 1D for the absorption hologram.

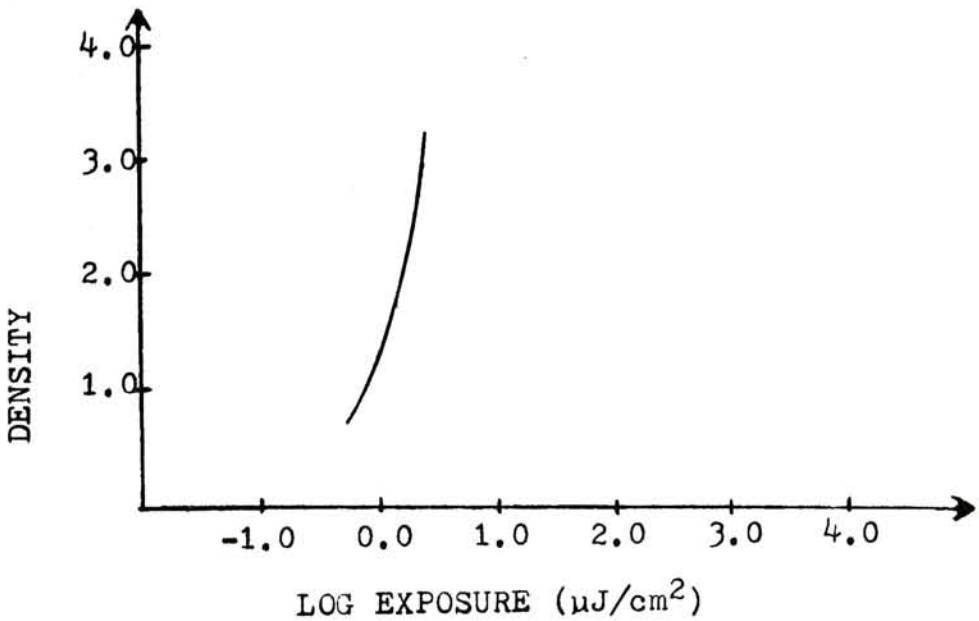

Fig. 1D. Density as a function of log exposure for Kodak high speed holographic plate.

This absorption hologram was then bleached in dry bromine vapor as described earlier. The diffraction efficiency is plotted as a function of density in Fig. 2D.

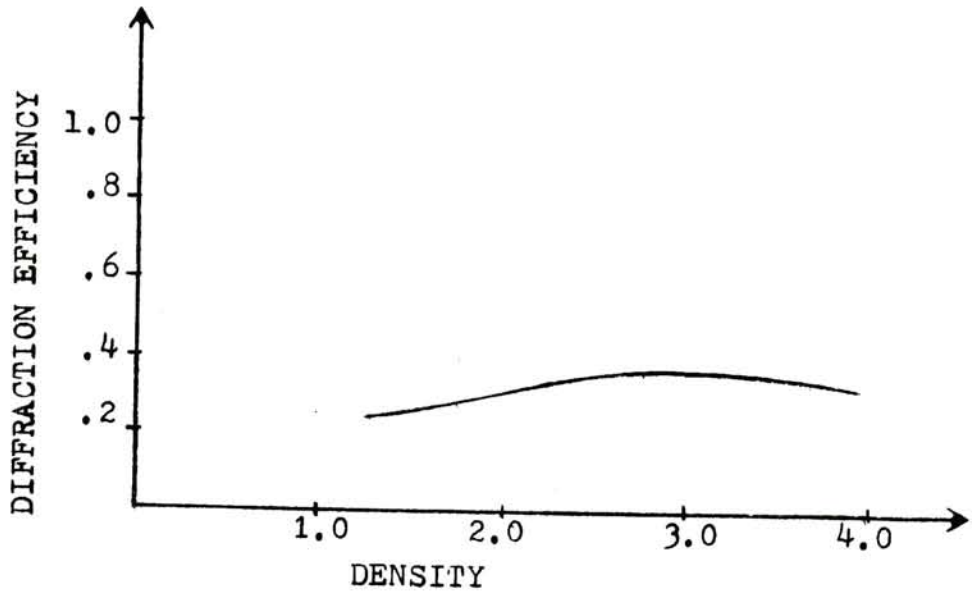

Fig. 2D. Diffraction efficiency as a function of density for Kodak high-speed holographic plates.

The images which resulted from this film-process combination were not as good as those obtained by reversal bleaching the Agfa 8E75 plates. This and the comparatively low diffraction efficiency could be attributed to the larger grain structure and the lower resolution of the Kodak high-speed plates.

APPENDIX E

Reflection Holography

For the purpose of demonstrating a hologram's ability to reconstruct a signals wavefront, reflection holograms were produced. A reflection hologram in constructed by having the reference wave and signal wave incident on opposite sides of the plate. This creates a standing wave irradiance pattern in the emulsion. When this plate is processed to a phase hologram, the fringes are planes of spatially modulated index of refraction in the plane parallel to the recording plate. These planes are on the order of a half a wavelength apart and can act as an interference filter to filter out the correct wavelength of light from white light for signal reconstruction.

To record the high frequency fringes, the apparatus has to have a high degree of mechanical stability. This aspect of reflection holograms makes them very difficult to produce. The apparatus used to make reflection holograms is shown in Fig. 1E and is schematically represented in Fig. 2E. This entire apparatus was covered with a box to isolate it from any air currents in the room.

Several attempts were made to record a reflection hologram in an entire 4" x 5" plate. Unless the path length of the signal wave from the beamsplitter to the plate is

Fig. 1E. Photograph of the apparatus used to make reflection holograms.

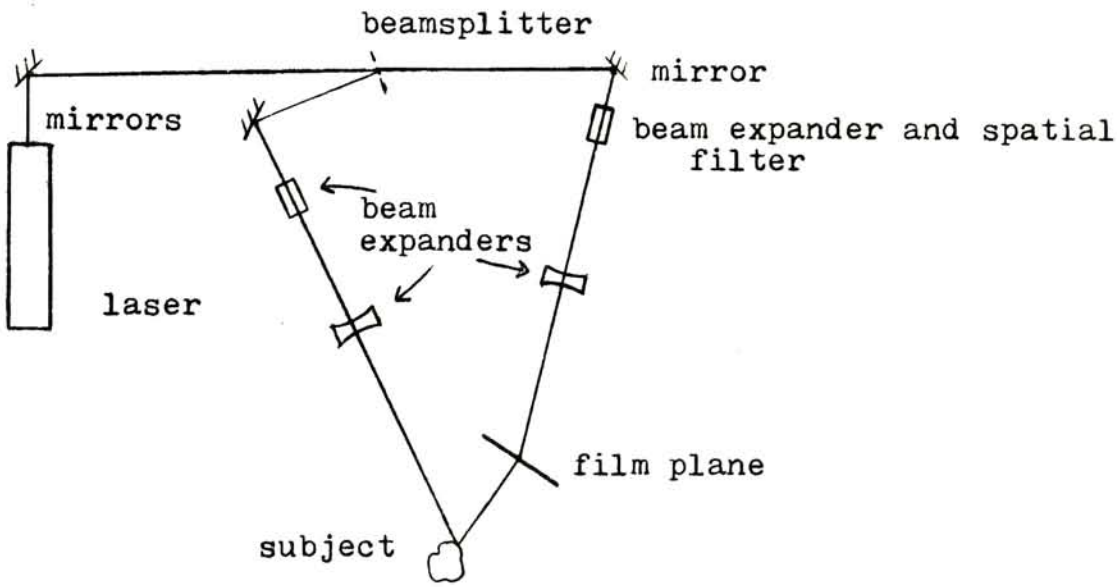

Fig. 2E. Schematic representation of apparatus in Fig. 1E.

very close ($\pm$ 1/8") to the reference wave path length from the beamsplitter to the plate, the fringes will not be recorded in the entire plate. This requires a very precise alignment of the apparatus to insure that all the components are on center. Optical path distances and directions should be set prior to the placement of the needed beam expanding optics.

The 8E75 Agfa holotest plates and the modified reversal bleach process, stated in the experimental section, were used to produce reflection holograms with good visibility. Exposures were approximately 100$\mu J/cm^2$, and the beam ratio was about 3:1.